Title	Transport characteristics of ramp-type YBa2Cu3O7-δ/PrBa2Cu3O7-y/YBa2Cu3O7-δ Josephson junctions
Author(s)	Sun, JL; Gao, J
Citation	Physical Review B (Condensed Matter and Materials Physics), 2000, v. 62 n. 2, p. 1457-1463
Issued Date	2000
URL	http://hdl.handle.net/10722/43303
Rights	Creative Commons: Attribution 3.0 Hong Kong License

Transport characteristics of ramp-type $YBa_2Cu_3O_{7-\delta}/PrBa_2Cu_3O_{7-y}/YBa_2Cu_3O_{7-\delta}$ Josephson junctions

J. L. Sun and J. Gao
Department of Physics, The University of Hong Kong, Pokfulam Road, Hong Kong
(Received 10 May 1999; revised manuscript received 14 September 1999)

The transport behaviors of $YBa_2Cu_3O_{7-\delta}/PrBa_2Cu_3O_{7-y}/YBa_2Cu_3O_{7-\delta}$ junctions with barrier thickness ranging from 6 to 30 nm were studied. In these junctions, the existence of a proximity layer was confirmed by the appearence of a temperature-dependent coherence length. The structure of the junctions changed from SNS to SNINS with increasing barrier thickness. It was found that the quasiparticles transport through a thin barrier by metallic conduction and through a thick barrier by tunneling conduction. In junctions with a moderate barrier thickness, we found a subgaplike feature in the conductance-voltage curves, which could be related to multiple Andreev reflection in a SNcNS Josephson junction. For junctions with a thick barrier, the dependence of conductance on temperature could be well fitted by the $T^{4/3}$ law. This suggested that the quasiparticles transport across a thick $PrBa_2Cu_3O_{7-y}$ barrier layer via two localized states in an inelastic tunneling process.

I. INTRODUCTION

High-T_c Josephson junctions with $PrBa_2Cu_3O_{7-y}$ (PrBCO) as barrier layer have been intensively investigated since they were first introduced in 1991.[1,2] PrBCO is selected as a barrier layer because of its small lattice mismatch with $YBa_2Cu_3O_{7-\delta}$ (YBCO), similar fabrication conditions as that of YBCO, and small interdiffusion at the YBCO/PrBCO interface. With PrBCO as a barrier material, the stationary properties of the junctions have been studied by several groups.[3–5] The temperature dependence of the critical current reported by different groups varied from quasilinear, $(1-T/T_c)^2$ to exponential dependence.[3,4,6] The divergence of these works is partly due to the complexity of the properties of PrBCO film. Currently, the transport behavior of charge carriers in PrBCO is a controversial topic. Transport in the bulk material of PrBCO was commonly described by variable-range hopping. However, Lee *et al.* reported the coexistence of nonmetallic hopping conduction with metallic Boltzmann transport on highly oriented PrBCO thin films deposited on $LaSrGaO_4$ substrate.[7] The hopping was assigned to the CuO_2 planes, while the metallic transport arises from the CuO chain structure. Recently superconductivity has been found in small bulk PrBCO samples grown by the traveling-solvent floating-zone method.[8] Kabasawa *et al.* studied the size effect on transport properties of PrBCO using planar-type junction specimens. Metallic transport behavior was observed for a small PrBCO bridge ($<0.2\ \mu$m).[9] From these experimental results, transport properties for junctions with different PrBCO barrier thickness are expected to be very different. To understand the dependence of junction properties on the barrier thickness, we studied the nonstationary as well as stationary properties of the junctions with different barrier thickness. Nonstationary properties of junctions have been studied by relatively few groups compared with the study of stationary properties.[10,11] The results in Ref. 10 indicated that both Cooper pairs and quasiparticle transport through PrBCO barriers are by a tunneling process, while subgap structures, resulting from multiple Andreev reflection, indicate the existence of a proximity layer in the barriers region.[11] In our experiment, the differences in physical properties of junctions with thin and thick barrier were analyzed and carefully compared. We found that there is a transition in the transport properties from metallic to insulating behavior for quasiparticles as the barrier thickness is increased.

II. EXPERIMENT

The geometry of a ramp-type junction and its detailed fabrication process were described in Ref. 12. Briefly, the YBCO electrodes and PrBCO barrier layer were epitaxially deposited on $SrTiO_3$ substrate using off-axis rf magnetron sputtering from stoichiometric targets. $SrTiO_3$ was selected as a substrate because of its small mismatch with YBCO in both lattice parameter and thermal expansion coefficients. Standard photolithographic techniques were employed in patterning the thin film into the desired structure. To minimize damage to the ramp edge of the base electrode, a moderate Ar-ion-beam milling rate as low as 5 nm/min was used. Because the outgrowth on the surface of the bottom electrode and insulating layers could be transferred onto the ramp edge during the ion milling process, the two bottom layers were prepared with very smooth surfaces free of outgrowth as shown by scanning electron microscopy (SEM). The microstructure of these junctions investigated by transmission electron microscopy (TEM) was described in previous works.[13,14] The epitaxy remained through all layers at the ramp region without the formation of big grain boundaries. Amorphous layer and secondary phases were not observed at the barrier interfaces. In this experiment, the thickness of the top and bottom of the YBCO electrodes was 100–150 nm. It has been reported that PrBCO barriers thinner than 6 nm thickness would contain pinholes,[15] so the minimum barrier thickness was chosen as 6 nm and the barrier thickness was varied from 6 to 30 nm with the ramp angle controlled to be 40°. Clear microwave-induced steps were observed in all the samples. *I-V* curves can be fitted using the resistively

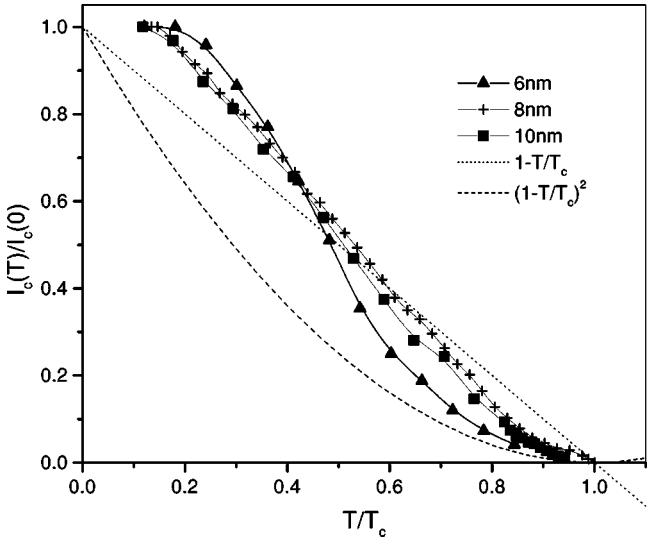

FIG. 1. Temperature dependence of the critical current for three junctions with different barrier thicknesses. $j_c \sim 10^5$ A cm^2, $R_n \sim 0.5\ \Omega$. The dotted and dashed lines are plots of $(1-T/T_c)$ and $(1-T/T_c)^2$, respectively.

shunted junction (RSJ) model including an excess current for the junctions with a thinner barrier. Finally, dynamic conductance has been calculated from the *I-V* curves of the junctions.

III. RESULTS

A. Critical current

The I_cR_n products of the junctions were in the range of 10^{-1} mV to a few mV at 10 K. The temperature dependence of the critical current can be divided into two groups as shown in Figs. 1 and 2, respectively. The three samples in the first group have barrier thickness from 6 to 10 nm and a relative large critical current density and a small resistivity. For the junctions in the second group, the temperature dependence of the normalized critical current follows $(1-T/T_c)^2$ near the critical temperature for all junctions. Almost half of the studied junctions follow this law in the whole temperature range.

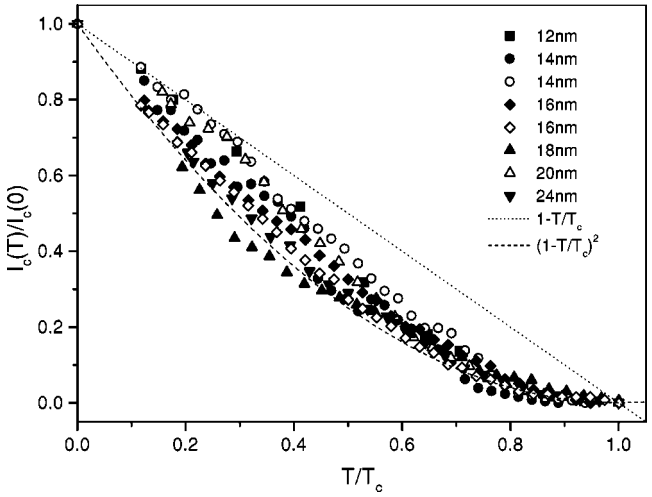

FIG. 2. Temperature dependence of critical current for junctions with different barrier thicknesses. $j_c \sim 10^4$ A cm^{-2}, $R_n \sim 1$–$2\ \Omega$. The dotted and dashed lines are plots of $(1-T/T_c)$ and $(1-T/T_c)^2$, respectively.

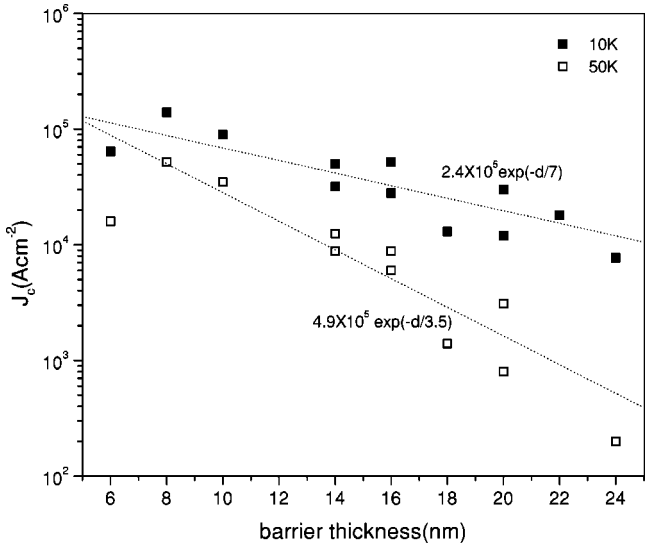

FIG. 3. Dependence of critical current on barrier thickness. The dotted lines are fitted to $j_c = j_{c0}e^{-d/\xi_n}$ with $j_{c0} = 2.4 \times 10^5$ A cm^{-2}, $\xi_n = 7$ nm at 10 K and $j_{c0} = 4.9 \times 10^5$ A cm^{-2}, $\xi_n = 3.5$ nm at 50 K.

The dependence of the critical current on the barrier thickness at 10 and 50 K is shown in Fig. 3. de Gennes proximity theory predicts that for a superconducting-normal-superconducting (SNS) junction, $j_c = j_{c0}e^{-d/\xi_n}$ over a broad range of temperature below T_c, with

$$j_{c0} = \frac{\pi|\Delta_i|^2}{2ek_BT_c\xi_{nd}\rho_n}.$$

d is the bridge length and Δ_i is the superconducting gap at the SN interface. The entire resistance is due to the normal interlayer N, $R_n = \rho_n d/A$. The experimental data were fitted by the above relation with $j_{c0} = 2.4 \times 10^5$ A cm^{-2}, $\xi_n = 7$ nm at 10 K and $j_{c0} = 4.9 \times 10^5$ A cm^{-2}, $\xi_n = 3.5$ nm at 50 K. The temperature dependence of the characteristic scaling length ξ_n is shown in Fig. 4. With the increase of temperature, ξ_n decreases monotonically. This temperature dependence of ξ_n indicates the existence of a proximity ef-

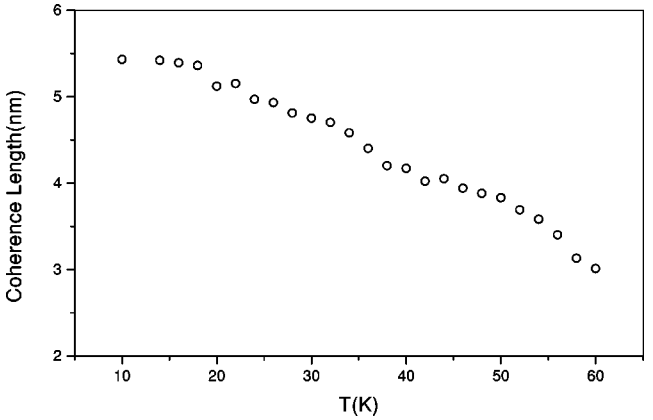

FIG. 4. Temperature dependence of the characteristic scaling length in the barrier.

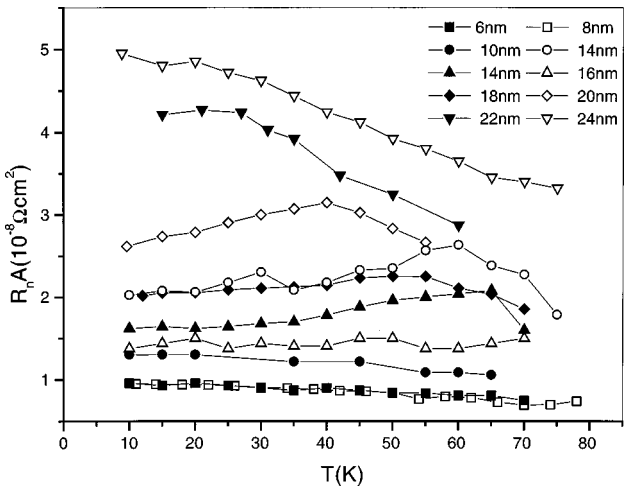

FIG. 5. Dependence of the characteristic resistance R_nA on temperature for junctions with different barrier thicknesses.

fect within the barrier layer. For a superconducting-insulating-superconducting (SIS) junction, ξ_n is independent of temperature. The ξ_n-T curve cannot be fitted with the T^{-1} or $T^{-1/2}$ temperature dependence expected for a normal metal proximity layer in the clean or dirty limit. This implies that the junction cannot be simply described as a SNS junction. As will be discussed later, the properties of the barrier layer are different in junctions with different barrier thickness.

B. Normal resistance of junctions

The R_nA product of junctions is of the order of $10^{-8}\Omega$ cm^2. The temperature dependence of R_nA for samples with different barrier thickness is plotted in Fig. 5. Great care should be taken when calculating R_n at high temperature because of thermal-activated resistivity in the weak-link region. The temperature dependence of R_n is different for junctions with varied barrier thickness. When the thickness is less than 10 nm, R_nA decreases slightly when the temperature is increased. In the samples with thickness more than 14 nm, a change in the slope of the curves with increasing temperature occurs. The R_nA product increases at low temperature but decreases at high temperature. The conductance $G_n=1/R_nA$ of the two samples with the largest thicknesses of 22 and 24 nm (corresponding to the uppermost two curves in Fig. 5) is fitted to $T^{4/3}$. The fitting at higher temperature is good as shown in Fig. 6 by solid symbols. The conductances taken near zero voltage are also plotted in this figure (open symbols). These data deviate from the $T^{4/3}$ relation below 40 K.

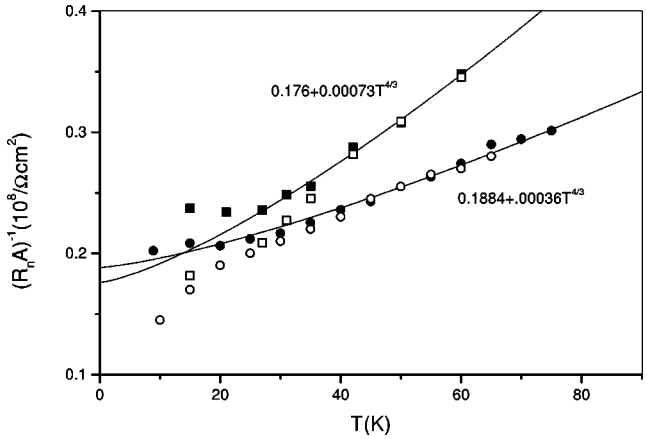

FIG. 6. The temperature dependence of conductance for two junctions with barrier thickness 22 nm (squares) and 24 nm (circles), respectively. The solid symbols represent the normal conductance of the junction taken at high voltage. The open ones represent the conductance taken near zero voltage. The solid lines are fitted to $T^{4/3}$.

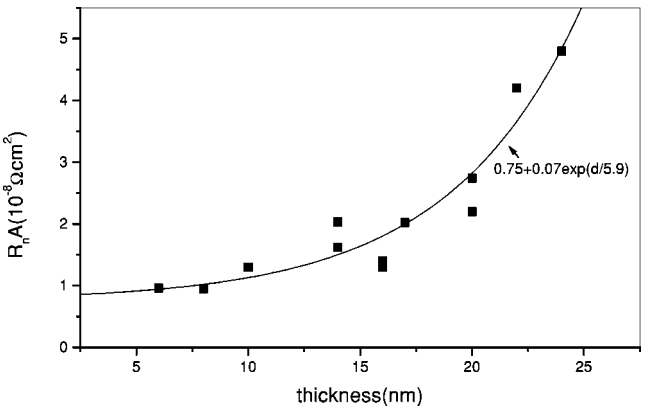

FIG. 7. Thickness dependence of R_nA of the junctions. $T=10$ K. The solid line is fitted to $R_nA=R_BA+\alpha e^{d/5.9}$ with $R_BA=7.5\times10^{-9}$ Ω cm^2, $\alpha=7\times10^{-10}$ Ω cm^2.

The R_nA dependence on thickness increases exponentially with an offset on the y axis as shown in Fig. 7. This offset implies an interface resistance $R_BA=7.5\times10^{-9}$ Ω cm^2 that is small in comparison with the normal resistance of the junctions.

The dependence of the critical current on the resistance of the junctions was also studied. As can be seen from Fig. 8, the data from junctions with barrier thickness less than 18 nm are distributed along the line $I_cR_n^{-1.9}$. For SNS structures with a barrier thickness $L\ll\xi_n$, one would expect $I_cR_n^{-2}$, whereas $I_cR_n^{-1}$ is expected for SNINS structure.[16,17] This implies that the junctions with a thin barrier possess a SNS structure.

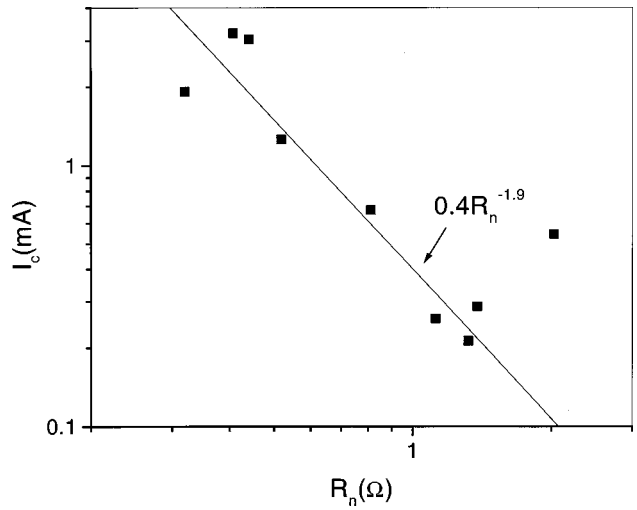

FIG. 8. Critical current as a function of the normal resistance of junctions at 10 K.

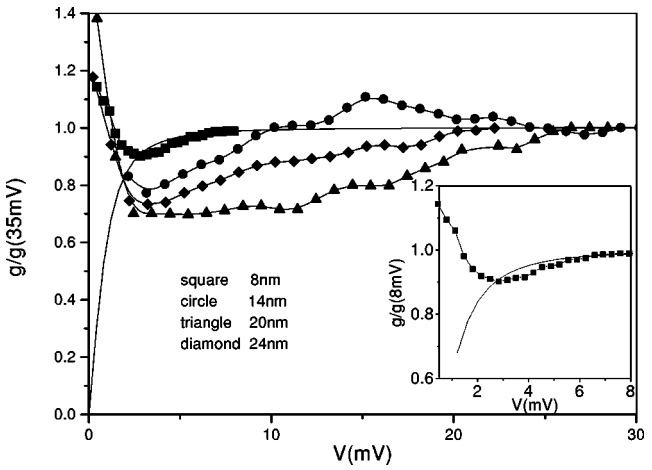

FIG. 9. Comparison of the dynamic conductance versus voltage with the RSJ model for junctions with different barrier thicknesses. The conductance is normalized to its value at 35 mV. The solid line without symbols represents a fit to the RSJ model with $I_c = 3$ mA, $R_n = 0.43\ \Omega$. The inset gives an enlarged plot for the junction with 8 nm PrBCO.

C. Dynamic conductance versus voltage

The dependence of the dynamic conductance $G_d = dI/dV$ on voltage changed dramatically for junctions with different barrier thickness. Although the small junction resistance and large current induced thermal effects make the measurement to higher voltage difficult for junctions with a thin barrier, it can still be inferred that G_d for samples with barrier thickness smaller than 10 nm reaches a constant value at small voltage (<10 mV). By contrast, in those junctions with a thicker barrier, G_d is a function of voltage up to 20 mV or even higher voltage. This is illustrated in Fig. 9. The dynamic conductance for the RSJ model, which assumes a constant normal resistance for each junction, is plotted for comparison. The deviation of the experimental data from the RSJ model near zero voltage is a reflection of ''round off'' on the I-V curve, which is caused by electrical noise in the

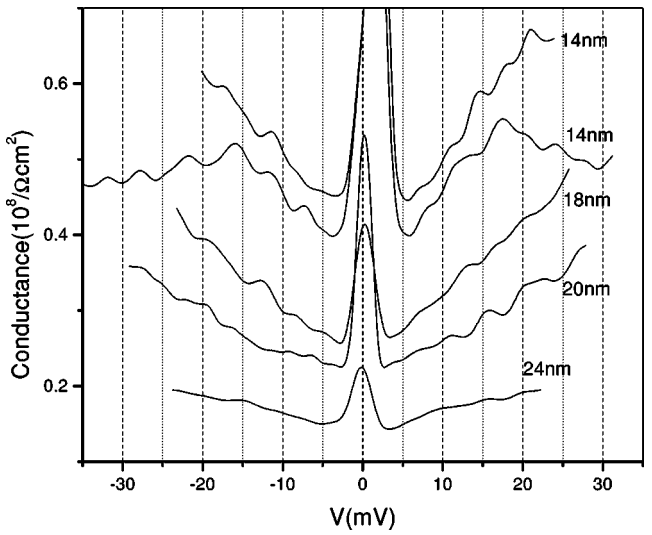

FIG. 10. Dynamic conductance vs temperature for junctions with different barrier thicknesses. The top curve is shifted 0.04 up for clarity.

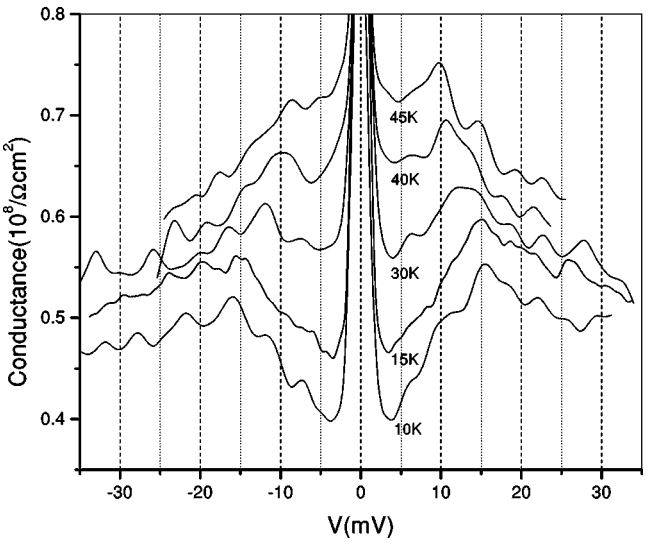

FIG. 11. Dynamic conductance at different temperatures for a junction with barrier thickness 14 nm. The curves are offset in the vertical direction for clarity.

I-V measurement. At higher voltage, some fine structures can be found on the curves. These fine structures are observed in the samples with thickness over 14 nm. Figure 10 shows G_d for junctions with different thicknesses at a temperature of about 10 K. The top two curves are for junctions with the same nominal barrier thickness 14 nm but different junction width (10 and 20 μm). The values of the two curves at the lower voltage overlap with each other, so one curve is shifted up 0.04 for clarity. From this figure, three peaks located at 12, 16, and 22 mV can be clearly seen for junctions with barrier thickness 14 nm. For other junctions similar peaks can also be observed. These peaks shift toward lower voltage with increasing temperature, as shown in Fig. 11.

IV. DISCUSSION

The variation of resistance with temperature and barrier thickness, and the dynamic conductance versus voltage, as well as the subgap structure in the G_d-V curves gave explicit signature to the properties of the junctions. Summarizing all these results, our junctions could be characterized as SNS structure when the barrier is thin, as SNINS structure with a thick barrier, and as SNcNS structure for a moderate thickness of barrier.

When the barrier thickness is less than 10 nm, the resistance of the junction is dominated by the interface resistance R_B as indicated by Fig. 7 and it decreases slightly at higher temperature. Thus, the normal resistance of junctions is independent of voltage as can be seen from Fig. 9. The V-I curves of these junctions assume standard RSJ behavior with an excess current. If we consider also the presence of the proximity layer, as indicated by the variation of the coherence length with temperature, then we can conclude that these junctions are best described as SNS structures.

In the junctions with a thick barrier, the properties of the junctions can be described by a SNINS structure. For transport by inelastic tunneling processes across an insulator layer

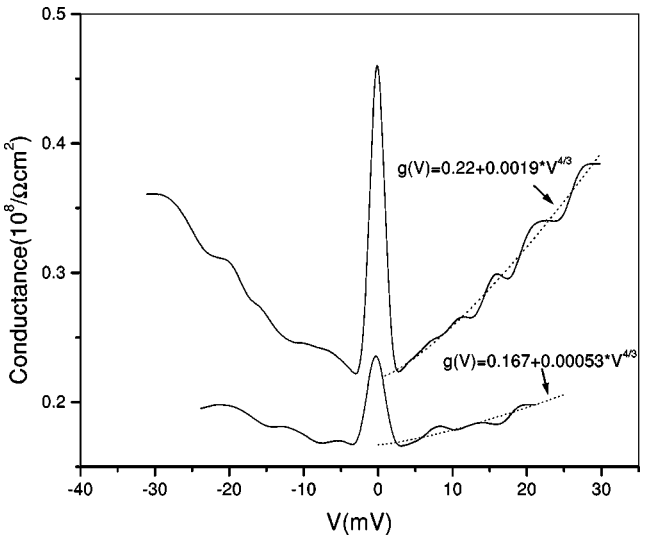

FIG. 12. The dynamic conductance of junction with barrier thickness 20 nm at 10 K (top) and 24 nm at 15 K (bottom). The dotted line is fitted with $V^{4/3}$.

containing two localized states, the conductance was given by Glazman and Matveev[18] as

$$G(T)=G_0+\alpha T^{4/3} \quad (eV \ll k_B T), \tag{1a}$$

$$G(V)=G_0+\alpha V^{4/3} \quad (eV \gg k_B T), \tag{1b}$$

where G_0 denotes temperature- and voltage-independent conductance due to direct or resonant tunneling via one localized state, α is a constant, and T is the temperature. Conductance in Eq. (1a) should be near zero-biased voltage as required by the inequality $eV \ll k_B T$. As shown in Fig. 6, the temperature dependence of conductance for the junctions with a thick barrier can be well fitted to Eq. (1a). The voltage dependence of the dynamic conductance for junctions with barrier thickness larger than 20 nm can also be fitted to Eq. (1b) at low temperature by superimposing a fine structure as mentioned above (Fig. 12). Conductance data taken near zero-biased voltage deviate from the relation of $T^{4/3}$ when the temperature is lower than 40 K (see Fig. 6). It should be pointed out that Eq. (1a) is developed for a system with normal metal as electrodes in which the density of states near the Fermi surface is temperature independent. In our situation, the electrodes are superconductors. The opening of an energy gap near the Fermi surface below the critical temperature is manifested by a decrease in the conductance of the system for small voltages $V<2\Delta(T)$, where $\Delta(T)$ is the energy gap of the superconducting electrodes.

The peak on the R-T curves shifts towards lower temperature as the thickness of the barrier increases (see Fig. 5). This is in agreement with the result given by Ref. 18. The temperature, at which the contribution made to the conductance by the second term in Eq. (1a) exceeds the contribution of the first term, is proportional to $\exp(-d/4a)$, where a is the radius of the localized state and d is the barrier thickness.

When the barrier thickness is not large enough to accommodate two localized states, the quasiparticles would tunnel through the barrier directly or resonant tunnel via one localized state. The resistance is expected to be temperature independent. This is the case for junctions with barrier thickness less than 16 nm. Previously, Yoshida and Nagano found that inelastic tunneling of quasiparticles via two localized states was the dominant process in PrBCO layers as thin as 5 nm.[19] We believe that this difference in scales may result from a difference in the structure of the junctions used in these two experiments. In the work of Ref. 19, the junction was formed by YBCO/PrBCO/Au. The carrier concentration (holes) in PrBCO is less than one-tenth that of YBCO as inferred from Hall effect measurements.[20] There may be a transition layer at the interface between YBCO and PrBCO where diffusion of carriers takes place. Thus the effective thickness of PrBCO is reduced in the YBCO/PrBCO/YBCO junctions used in our experiment. The slight increase of R_n with temperature may be attributed to the proximity layer formed at the YBCO/PrBCO interface. The total normal resistance of the junction is $R_n=R_B+R_p$ where R_p is the resistance of the proximity layer.

A SNcNS model could be applicable to our junctions with moderate barrier thickness to explain the subgap structures observed in these junctions. The SNcNS structure was proposed to describe the conventional junction Nb-AlO_x-Nb, where N represents the proximity layer next to the insulating layer.[21] When the insulator layer is not thick enough so that its energy barrier is low, the insulating layer could be viewed as a small constriction c between SN and NS with a certain energy barrier. The small constriction c is assumed to be a small orifice of radius a [$a \ll \min(l_n, l_s) \ll \xi_{n,s}$, where $l_{n,s}$ and $\xi_{n,s}$ are the mean free path and coherence length in S and N]. This might be the case for our samples with a moderate PrBCO layer. The localized states in the barrier layer could act as constrictions which communicate between SN and NS banks. In a SNcNS junction, according to the work of Aminov *et al.*,[21] a complicated peak structure would appear in the dynamic conductance-voltage curve due to the multiple Andreev reflection. With a finite energy barrier height in the constriction ($Z=H/\hbar v_f \neq 0$; H is the energy barrier height in the constriction, and v_f is Fermi velocity), the additional order parameter in the proximity layer would result in a complex peak and dip structure at the voltage $V_n=2\Delta_n/(en)$, $V_n=(\Delta_s-\Delta_n)/(en)$, $V_n=(\Delta_s+\Delta_n)/(en)$, and $V_n=2\Delta_s/(en)$ on the G_d-V curve in the whole measured temperature range. Here Δ_s and Δ_n denote the order parameters for the proximity layer at the SN interface and Nc interface, respectively. The subgap structures in our experiment are too complex to distinguish the peaks from each other. Referring to the result in Ref. 21, the peak with the highest intensity is $2\Delta_n/e$. If we take the peaks at 16 and 22 mV in Fig. 10 as corresponding to $2\Delta_n/e$ and $(\Delta_s+\Delta_n)/e$, we derive a gap value of $\Delta_s=14$ meV and $\Delta_n=8$ meV for the proximity N layer at the superconducting electrode side and insulator side, respectively. With the increase of temperature, the difference between Δ_n and Δ_s decreases; $V=2\Delta_n/e$ and $V=(\Delta_s+\Delta_n)/e$ merge as one peak.

Interface parameters $\gamma=(N_n/N_s)(D_n/D_s)^{1/2}$ for our junctions have been deduced from the temperature dependence of Δ_n by assuming that the temperature dependence of $\Delta_n(T)$ follows that of $\Delta_i(T)$, where Δ_i is the intrinsic depressed order parameter at the SN interface on the S side. At the boundary of the superconductor and normal metal, the intrinsic depression of the order parameter at the S side of a SN interface is derived for a dirty superconductor from the

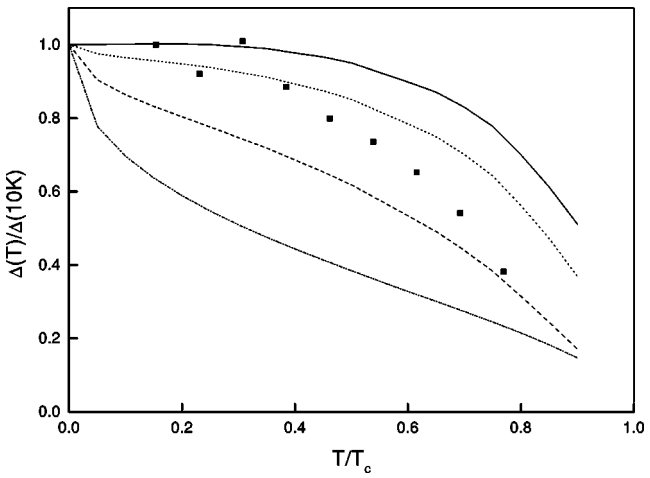

FIG. 13. Temperature dependence of the highest peak position in Fig. 11 for barrier 14 nm (scattered squares) normalized to its value at 10 K. The solid line represents the bulk YBCO order parameter. Three dotted lines are fitted with $\gamma=0.1,\ 0.4,\ 1$, respectively, from top to bottom. $\gamma=(N_n/N_s)(D_n/D_s)^{1/2}$.

phenomenological Ginzburg-Landau theory which generally applies at temperatures down to $0.3T_c$:[22]

$$\left(\frac{\Delta_i}{\Delta_0}\right)^2=1+\left(\frac{\xi_{sd}}{b_i}\right)^2-\left[\left(\frac{\xi_{sd}}{b_i}\right)^4+2\left(\frac{\xi_{sd}}{b_i}\right)^2\right]^{1/2} \tag{2}$$

and

$$\frac{\xi_{sd}}{b_i}=\frac{\rho_s\xi_{sd}}{\rho_n\xi_{nd}}=\frac{\pi}{2}\gamma\left(\frac{T}{T_c-T}\right), \tag{3}$$

where Δ_0 is the order parameter for bulk superconducting electrodes, and $\xi_{sd,nd}$ and $D_{s,n}$ are the temperature-dependent Ginzburg-Landau coherence length and coefficient of carrier diffusion in superconducting and normal barriers, respectively. The parameter b_i is the extrapolation length of the order parameter in the N layer at the SN interface. γ describes the depression of order parameter of YBCO at the SN interface. The temperature dependence of $2\Delta_n/e$ (corresponding to the highest peak position in Fig. 11) for junctions with barrier 14 nm is illustrated in Fig. 13 as scattered solid squares. The solid line in the figure is the order parameter for bulk YBCO normalized to its value at $T=0$.[23] The three dashed lines are the value of Δ_i calculated from the above equations with the same normalization using $\gamma=0.1,\ 0.4,\ 1$, respectively. Comparing the experimental data with the theoretical result, γ is estimated to be within 0.1–0.4.

Another interface parameter $\gamma_B=R_B/\rho_n\xi_n$ has also been evaluated for our junctions. With the value of γ and the result $\Delta_n/\Delta_s\approx 0.6$, according to Fig. 1 in Ref. 21, γ_B is estimated to be less than 2 in our junctions. Thus, the interface resistance R_B is not larger than the resistance of the normal layer. This is consistent with the result inferred from the y axis offset in Fig. 7 which shows an interface resistance of about $10^{-9}\ \Omega\ \mathrm{cm}^2$. Such a value of interface resistance is comparable with those given by other groups.[24] This accounts for the temperature-insensitive behavior of the normal resistance for junctions with a thinner barrier. γ and γ_B have been calculated for YBCO and PrBCO bulk material from typical values of coherence length and coefficient of diffusion, and have been given values of 10^{-4} and 10^{-1}, respectively.[25] These are much smaller than those estimated from our experimental results. This leads us to conclude that the physical properties of a PrBCO thin film on a nanoscale are much different from those for the bulk material.

V. CONCLUSION

By studying nonstationary properties of junctions, informative results were obtained. Usually both Cooper pairs and quasiparticles are considered to tunnel across the PrBCO barrier. From the results of our experiment, this is true only for junctions with a thick barrier. The junction structures can be divided into three types related to their barrier thickness: SNS, SNcNS, and SNINS. In our experiment, evidence for the existence of a proximity layer is clearly seen from the subgap structure in the dynamic conductance curve. The subgap peaks were more complex than expected from the simple expression $2\Delta/en$, $n=1,2,3,\ldots$, and are attributed to multiple Andreev reflection in Josephson junctions with a SNcNS structure. At medium thickness, constrictions between proximity layers dominate in the barrier region and are indicated by the gap structure. The constriction might be a localized state in the PrBCO layer. The gap feature fades away with an increase of the barrier thickness and the quasiparticle transport across the barrier falls into a tunneling regime. Further work is needed to be done to clarify the nature of the constriction. Further study is also required to clarify if the proximity layer is formed by a thin PrBCO layer or a thin YBCO layer near the SN interface with a degraded T_c, or a mixture of both.

ACKNOWLEDGMENTS

This work has been supported by the Research Grants Council (RGC) of Hong Kong and the Committee on Research and Conference Grants (CRCG) of The University of Hong Kong. The authors would like to thank Dr. W. H. Tang and L. F. Gong for their helpful discussions.

[1] J. Gao, W. A. M. Aarnink, G. J. Gerritsma, and H. Rogalla, Physica C **171**, 126 (1990).

[2] J. Gao, Yu. M. Boguslavskij, B. B. G. Klopman, D. Terpstra, R. Wijbrans, G. J. Gerritsma, and H. Rogalla, Appl. Phys. Lett. **59**, 2754 (1991).

[3] Yu. M. Boguslavskij, J. Gao, A. J. H. M. Rijnders, D. Terpstra, G. J. Gerritsma, and H. Rogalla, Physica C **194**, 268 (1992).

[4] M. I. Faley, U. Poppe, H. Solter, C. L. Jia, M. Siegel, and K. Urban, Appl. Phys. Lett. **63**, 2138 (1993).

[5] J. B. Barner, B. D. Hunt, M. C. Foote, W. T. Pike, and R. P. Vasqueez, Physica C **207**, 381 (1993).

[6] Tatsunori Hashimoto, Masayuki Sagoi, Yoshihisa Mizutani Jiro

Yoshida, and Koichi Mizushima, Appl. Phys. Lett. **60**, 1756 (1992).
[7] Mark Lee, Y. Suzuki, and T. H. Geballe, Phys. Rev. B **51**, 15 619 (1995).
[8] Zhigang Zou, Jinhua Ye, Kunihiko Oka, and Yoshikazu Nishihara, Phys. Rev. Lett. **80**, 1074 (1998).
[9] U. Kabasawa, Y. Tarutani, M. Okamoto, T. Fukazawa, A. Tsukamoto, M. Hiratani, and K. Takagi, Phys. Rev. Lett. **70**, 1700 (1993).
[10] M. A. J. Verhoeven, G. J. Gerritsma, H. Rogalla, and A. A. Golubov, Appl. Phys. Lett. **69**, 848 (1996).
[11] E. Polturak, G. Koren, D. Cohen, and E. Aharoni, Phys. Rev. B **47**, 5270 (1993).
[12] J. Gao, Yu. M. Boguslavskij, B. B. G. Klopman, D. Terpstra, R. Wijbrans, G. J. Gerritsma, and H. Rogalla, J. Appl. Phys. **72**, 575 (1992).
[13] Y. Yang, J. Gao, J. L. Sun, T. C. Chui, and L. Li, Physica C **300**, 151 (1998).
[14] J. Gao, Y. Yang, and J. L. Sun, IEEE. Trans. Appl. Supercond. **9**, 3145 (1999).
[15] M. A. J. Verhoeven, R. Moerman, M. E. Bijlsma, A. J. H. M. Rijnders, D. H. A. Blnak, G. J. Gerritsma, and H. Rogalla, Appl. Phys. Lett. **68**, 1276 (1996).
[16] M. Yu. Kupriyanov and K. K. Likharev, IEEE Trans. Magn. **27**, 2460 (1991).
[17] K. K. Likharev, Rev. Mod. Phys. **51**, 101 (1979).
[18] L. I. Glazman and K. A. Matveev, Zh. Éksp. Teor. Fiz. **94**, 332 (1988) [Sov. Phys. JETP **67**, 1276 (1988)].
[19] J. Yoshida and T. Nagano, Phys. Rev. B **55**, 11 860 (1997).
[20] A. Matsuda, K. Kinoshita, T. Ishii, H. Shibata, T. Watanabe, and T. Yamada, Phys. Rev. B **38**, 2910 (1988).
[21] B. A. Aminov, A. A. Golubov, and M. Yu. Kupriyanov, Phys. Rev. B **53**, 365 (1996).
[22] K. A. Delin and A. W. Kleinsasser, Supercond. Sci. Technol. **9**, 227 (1996).
[23] *Concise Encyclopedia of Magnetic & Superconducting Materials*, edited by J. E. Evetts (Pergamon Press, New York, 1992).
[24] L. Antognazza, S. J. Berkowitz, T. H. Geballe, and K. Char, Phys. Rev. B **51**, 8560 (1995).
[25] Y. M. Boguslavskij, J. Gao, A. J. L. H. M. Rijnders, D. Terpstra, G. J. Gerritsma, and H. Rogalla, IEEE Trans. Appl. Supercond. **3**, 2034 (1993).